United Kingdom Infrared Telescope's Spectrograph Observations of Human-Made Space Objects

Brent Buckalew[(1)], Kira Abercromby[(2)], Susan Lederer[(3)], Heather Cowardin[(4)], James Frith[(4)],

[(1)]JACOBS, 2224 Bay Area Blvd. Houston, TX 77058, USA, brent.a.buckalew@nasa.gov
[(2)]California Polytechnic State University, San Luis Obispo, kabercro@calpoly.edu
[(3)]NASA JSC, 2101 NASA Parkway, XI411, Houston, TX 77058, USA, susan.m.lederer@nasa.gov
[(4)]JACOBS JETS, University of Texas El Paso, 2224 Bay Area Blvd. Houston, TX 77058, USA

ABSTRACT

Presented here are the results of the United Kingdom Infrared Telescope (UKIRT) spectral observations of 17 human-made space objects (spacecraft, rocket bodies, and debris) taken in 2015. The remotely collected data are compared to the laboratory-collected reflectance data on typical spacecraft materials; thereby general materials are identified. These results highlight the usefulness of observations in the infrared by focusing on features from hydrocarbons and silicon. The model results of the spacecraft spectra show distinct features due to solar panels. These results show that the laboratory data in its current state gives excellent indications as to the nature of the surface materials on spacecraft. The model fits to rocket bodies and debris did not do as well, indicating a potential gap in the current methodology. To produce more reliable results for all space objects, we conclude with future work necessary to give logical results for both rocket bodies and debris.

1 INTRODUCTION

One of the roles of the NASA Orbital Debris Program Office at Johnson Space Center (JSC) is to characterize the debris environment through the assessment of the physical properties (type, mass, density, and size) of objects in orbit. Knowledge of the geosynchronous orbit (GEO) debris environment, in particular, can be used to determine the hazard probability at specific GEO altitudes and aid predictions of the future environment. Currently, an optical size is calculated using an assumed albedo for an object and its intensity measurement. However, identification of specific material type or types could improve albedo accuracy and yield a more accurate size estimate for the debris piece. Using spectroscopy, it is possible to determine the surface materials of space objects.

In this paper, we discuss the observations and data reduction of the spectra obtained as well as the laboratory spectra of various spacecraft materials. Next, we detail the spectral unmixing algorithm used to compare the observed spectra with the laboratory spectra. Then, we present our findings by highlighting our results for a spacecraft, debris, and rocket body. We follow these results with a comparison of stitched versus single order spectra and a comparison of these data presented here with those presented in previous studies.

2 DATA COLLECTION AND REDUCTION

2.1 Telescope Observations

Observations of orbital objects were taken with the 3.8-meter telescope at the United Kingdom Infrared Telescope (UKIRT) using the UKIRT 1-5 micron Imager Spectrometer (UIST) [1] instrument on 17-26 March 2015, 9-14 April 2015, 16-17 April 2015, 20-21 April 2015, and 24-27 April 2015. UIST was used in spectroscopy mode, and the slit width was 4 pixels (~0.48″). The data from the nights reported herein were spectrophotometric. In this configuration, the instrument provides a spectral resolution ($\lambda/\Delta\lambda$) of 320 for the IJ (0.86-1.42 microns) grism, of 450 for the JH (1.13-1.9 microns) grism, and of 500 for the HK (1.4-2.51 microns) grism. Signal-to-noise values of the data obtained are contingent on the brightness of the object at the time of observation, the total integration time, and the atmospheric conditions at the summit. The signal-to-noise values for most objects observed with this instrument are attainable in excess of 100, given good viewing conditions.

Over the course of these observations, spectral data were acquired on a subset of cataloged GEO targets from the U.S. Space Surveillance Network (SSN) database. These objects included spacecraft, rocket bodies, and orbital debris (see Tab. 1 for a summary of all observations). In two cases, SSN 14234 and SSN 27400 were observed in both March and April 2015. In 10 cases, individual objects were observed on multiple nights in the same month. During the course of a night's observation campaign, calibration data were acquired including flats, arc lamps (wavelength calibration), atmospheric standards (telluric feature removal), and solar analogs (for relative reflectance ratios). Typically, exposure time sets for the SSN objects were 60 seconds placed in five pairs (for a total of 10 exposures), where the object was shifted 1 arcsecond up and down the slit (necessary for sky emission removal and bias/dark removal) for a given slit pair.

Proc. 7th European Conference on Space Debris, Darmstadt, Germany, 18–21 April 2017, published by the ESA Space Debris Office
Ed. T. Flohrer & F. Schmitz, (http://spacedebris2017.sdo.esoc.esa.int, June 2017)

Table 1. UKIRT UIST Observation Summary

SSN	Common Names	International Designator	17-26 March 2015	9-14, 16-17, 20-21, & 24-27 April 2015
08832	TITAN 3C TRANSTAGE DEB	1976-023J		X
11669	OPS 6393 (FLTSATCOM 3)	1980-004A		X
12855	SBS 2	1981-096A		X
13431	ANIK D-1	1982-082A		X
14234	ARABSAT 1DR (TELSTAR 3A)	1983-077A	X	X
15383	ARABSAT 1-D (ANIK D-2)	1984-113B		X
15385	SPACENET 2	1984-114A		X
16274	MORELOS 2	1985-109B		X
19751	COSMOS 1989 (ETALON 1)	1989-001C		X
20026	COSMOS 2024 (ETALON 2)	1989-039C		X
20558	ASIASAT 1	1990-030A		X
20570	NEWSAT-1 (PALAPA B2R)	1990-034A		X
21648	COSMOS 2054 DEB	1989-101G		X
23185	APSTAR1	1994-043A	X	
23615	IUS R/B (2)	1995-035D		X
27400	ASTRA 3A	2002-015B	X	X
39688	CTS DEBRIS (ARRAY COVER)	1976-004E	X	

The data were reduced using Starlink [3] and recalibrated at NASA\JSC using ORAC-DR©, see [4] for details on post-processing.

Once the above steps were completed, the relative reflectance ratio spectra of the objects were produced. These images were produced by ratioing the object and solar analog star [5] that was visible during the observation period. To insure sky conditions are completely removed from the image, both the object spectra and solar analog spectra were ratioed by the standard star spectra closest in time and position to the object observations. This procedure gives us a final ratio of the target to solar analog where the telluric (*i.e.*, atmospheric) features have been minimized. An example of this ratio can be found in Fig. 1.

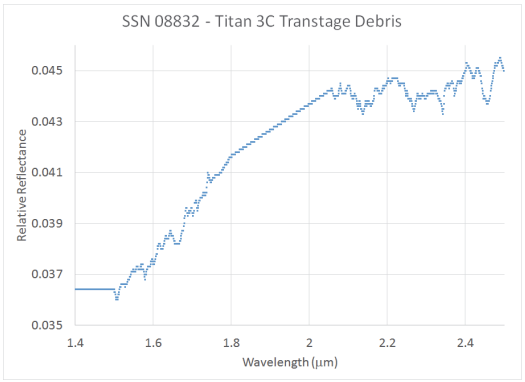

Figure 1. SSN 8832 spectral data acquired 13 April 2015 ratioed to the solar analog star SA 107-684. The y-axis is relative reflectance, and the x-axis is wavelength in microns. The smooth line (e.g., between 1.8 and 2.0 μm) is indicative of the removal of the residuals left over from removing telluric features. The removal of these residuals aided with the running of the spectral unmixing algorithm described below.

2.2 Laboratory Data

In order to quantify the spectral observations of the telescopic data, laboratory spectra were acquired to provide baseline measurements of known spacecraft materials. An Analytical Spectral Device field spectrometer that has a wavelength range from 0.3 to 2.5 microns (μm) with a resolution of 10 nanometers at a wavelength of 2 μm and 717 channels was used to obtain the laboratory measurements. From these laboratory measurements, a database of more than 300 common spacecraft materials reflectance spectra was assembled. The spectral laboratory data are maintained and updated via a NASA Spectral Database at NASA\JSC**;** see ref [2]. For the analysis done in support of this paper, a subset of materials from the NASA Spectral Database and additional materials not in the NASA Spectral Database, courtesy of K. Abercromby, were investigated. The materials used for the comparisons include exposed, manufacture samples, and pre-flight materials used for various spacecraft.

When collecting data in a laboratory, a white reference is measured and compared to the material spectrum such that the resulting spectrum is called an absolute reflectance measurement that is on the scale of zero to one. However, there is not such an absolute reflectance standard at the same distance and orientation of each of the satellites. Therefore, the data are considered as relative reflectances. In these cases, the overall shape of the spectrum and the absorption feature's strength and location are used to determine material type and not the percent reflectivity. In order to provide comparisons between two or more objects, a scaling factor is applied for all comparisons used throughout the paper.

3 SPECTRAL UNMIXING

Spectral unmixing is the process of inverting material proportions from a combined spectrum that has distinct components that are linearly mixed. Rapp [6] developed a Constrained Linear Least Squares (CLLS) model with the application of unmixing reflectance spectral data of orbiting objects. Spectra are added linearly according to the proportion represented on the surface of the object. Considering orientation of incident light and the object, the full equation defining the combined spectrum in terms of orientation [6, 7] is:

$$S_{combined} = \sum_{i=1}^{n} p_i B_i S_i + N \quad (1)$$

where S is a spectrum, i is an index representing the i^{th} material, p is the material proportion of the full spectrum, N is noise, and B_i is the orientation coefficient for the i^{th} material. Equation 1 is still an approximation, however, as the orientation can change the spectrum. It should be noted that $S_{combined}$ and S_i can be represented as very long vectors, with reflectance values at each of the measured wavelengths. This allows an expansion into a vector math representation:

$$\vec{S}_{combined} = p_1 B_1 \overrightarrow{S_1} + \cdots + p_n B_n \overrightarrow{S_n} + \vec{N} \quad (2)$$

where p_i and B_i are both scalars, making it quite easy to restate this as a matrix multiplication problem with a known solution:

$$S_c = SA. \quad (3)$$

Unfortunately, the matrix S is not square so it cannot be truly inverted to solve directly for A so a pseudo-inverse can be used. When applied to this problem this inverse is known as a least-squares optimization:

$$S^T S_c = S^T S A \quad (4)$$

Multiplying both sides by S^T creates a square matrix that is guaranteed to be invertible:

$$(S^T S)^{-1} S^T S_c = A \quad (5)$$

This function minimizes Equation 5 and provides a beginning point for the solution to the unmixing problem. Testing this solution, for some combined spectra the unmixer returned negative proportion values, which is physically impossible. This is because the model is trying to match shape and subtracting materials can be the same as adding in terms of the final result. To rectify this issue a constrained least squares function was used,

MATLAB's built in *lsqnonneg* function. The function uses a modified Lagrange multiplier method to solve the constrained problem. By reframing this as a vector problem, and recognizing it as a minimization problem, it becomes clear that the Lagrange solution is solving the constrained minimization problem:

$$f = (S_c - SA) \;\; A \geq 0 \tag{6}$$

This is solved for the specific $A \geq 0$ case by the *lsqnonneg* function. To maintain the constraint using a Lagrange multiplier method, the function first calculates the least squares solution, including negative solutions. It then uses those solutions to create a vector of logicals defining which solutions are negative, and need to be corrected. This vector becomes the Lagrange multiplier, and the optimization is performed. This process is repeated until an optimum solution is found.

To estimate the error in the results when unknown spectra are unmixed, the difference between the original and unmixed spectra is calculated (called the residual). Since a vector approximation method is used to calculate the best unmixing solution, the norm is calculated, and used for error. This area is then used to calculate the error based on the difference in area.

$$E = \frac{Norm_{diff}}{Norm_{orig}} = \frac{\sqrt{S_{diff}^T S_{diff}}}{\sqrt{S_c^T S_c}} \tag{7}$$

This error estimation gives a percentage error, and gives an estimation of the cut-off point of significant figures in the output. This model takes all the materials supplied and creates the best, combined spectrum based on the above method.

4 RESULTS

4.1 Spacecraft

The remotely collected data are compared to the laboratory-collected reflectance data on typical spacecraft materials; thereby general materials are identified but not specific types. Each spectral image shown contains the remote data on the object and the CLLS spectrum. In addition, a simple subtraction between the two spectra is also shown on the plots. This difference is calculated at each wavelength. The overall error (shown in the calculations in the previous section) is listed in the figure captions.

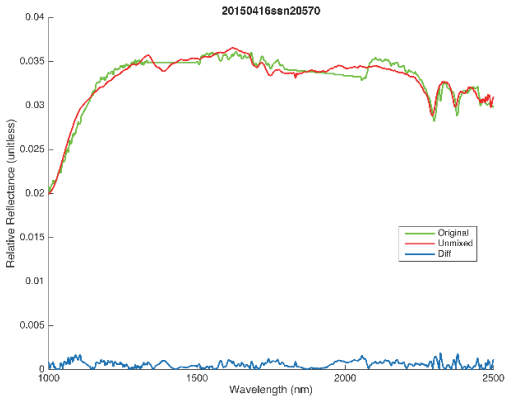

Figure 2. Spectral data over the IJ and HK grisms from SSN20570, an HS 376 bus. Green line is the original data, red line is the model fit to the data, and blue is the difference between the green and red lines. Each grism result was modeled separately. The percent error is 1.7% for IJ and 1.8% for HK.

Figure 3. Palapa-B image. This is an artist's rendition of an HS 376 communication satellite. Ref: http://space.skyrocket.de/doc_sdat/palapa-b.htm.

Spectral data on object SSN20570 (NEWSAT-1 [PALAPA B2R]) is shown in Fig. 2. The spectral data from the IJ grism and HK grism are plotted on the same figure. Both model data and the remote data are scaled such that their reflectances are compared. The matching materials used in CLLS were multi-layered insulation (MLI), solar cell, anodized aluminum (Al), Inconel, white paint, and exposed white paint. The model fits the original data to 1.7% for the IJ grism and 1.8% for the HK grism. These errors are typical for spacecraft fits. Solar cells have a band gap feature near 1100 nm, as seen in the original and unmixed data in Fig. 2. These results are consistent with the satellite design, which is a cylindrical bus-type covered in solar cells, similar to Fig. 3.

In addition to the solar cell feature, common features due to carbon-hydrogen (C-H) are seen near 1700 nm and 2400 nm in both the CLLS model and remote data. Also, the laboratory data tend to have some of the water features present (water features would be near 1400 nm and 1900 nm); however, the remote data have them completely removed due to the amount of water in the atmosphere. Thus, those water feature regimes will never agree with the CLLS model in any of the figures shown. In future work, the intent is to remove the features from the laboratory data and redo the comparison.

The best-fit spectra were that for the HK grism data of SSN 16274 (MORELOS 2). MORELOS 2 is an HS 376 like that depicted in Fig. 3. The fit for the MORELOS data is found in Fig. 4. The percentage error is 0.008% for the data taken on 24 April and 0.01% for the data taken on 16 April. Several of the key points discussed with the spectra of NEWSAT-1 can be reiterated here. Please see above for the prominent features discussed.

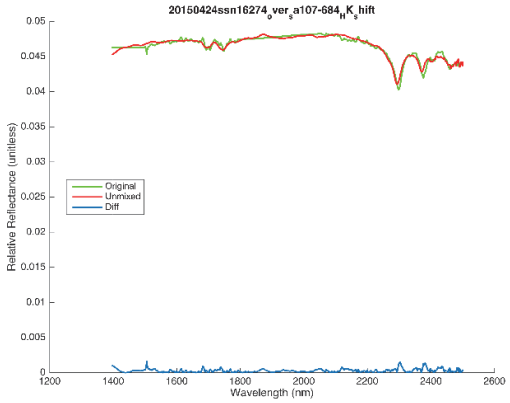

Figure 4. Spectral data from SSN16274, MORELOS 2 (an HS 376), with the HK grism. Green line is the original data, red line is the model fit to the data, and blue is the difference between the green and red lines. The percent error is 0.008%. These spectra and the features are similar to those found in Fig. 2.

4.2 Debris

Object SSN21648 (COSMOS 2054 debris) did not compare well to the CLLS model as shown in Fig. 5. The data are effectively flat with no obvious absorption features; the majority of debris spectra seen in this study and within the study using Infrared Telescope Facility data [7] are similar. The percent error for this fit of the 21648 data is 10.6%. Currently, the spectral library of materials has no information on ejected materials from satellites due to explosions or collisions. More material information is necessary to give any material identification from actual orbital debris.

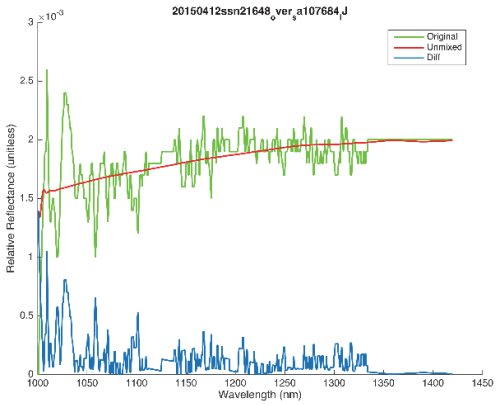

Figure 5. Spectral data from SSN21648, a debris piece from COSMOS 2054, with the IJ grism. Green line is the original data, red line is the model fit to the data, and blue is the difference between the green and red lines. The percent error is 10.6%. Debris typically have a flat composition. The spectral library of materials currently does not have the necessary knowledge to deal with these objects.

The CLLS had the hardest time matching materials with the orbital debris pieces. Two of the three debris pieces had some of the worse fits based on percentage errors. The CLLS model did not have materials in the database to match the debris pieces. Future work with the model must have contributions that address what happens with materials as well as chemical/physical changes from ejected debris. For the COSMOS 2054 debris, Al was the dominant match. In fact, SSN08832 (Titan Transtage 3C debris) and SSN 39688 (CTS debris [Array Cover]) all had fits with Al as a dominant material.

In some spectra (e.g., one of the April 2015 spectra of SSN08832), the materials fit with the CLLS model contains a contribution of solar cell emission. The authors think that solar panels are not in these objects. We think that some material with similar spectral response is contributing to the relative reflectance spectra that are not in the database nor in the model. For example, green paint on the nozzle of a Titan Transtage gives a similar spectral response to a solar cell (H. Cowardin, private communication). Such green paint absolute reflectances were not available when these analyses were completed. Again, future work is required to make the model more robust to handle the spectra of all debris.

4.3 Rocket Body

The results of the one rocket body, SSN23615, are shown in Fig. 6. SSN23615 is an Inertial Upper Stage (IUS) rocket body and is shown in Fig. 7. Four spectra were taken of this object on 17 and 20 April. The JH grism was observed on both nights. The CLLS model was able to detect the C-H features and the general slope to within

3.2%, 3.8%/5.2%, and 2.7% for the IJ, JH, and HK grism spectra. While solar cells are not found on the rocket body, the HK grism and IJ grism results are best fit with a solar cell as one of the components. Again, similar to the issues with SSN08832, these absorption features are correlated to solar cells but based on a priori knowledge of the rocket body, we know that such solar cells are not present. Based on work from H. Cowardin (private communication), specific paints have similar absorption features that are comparable to the solar cell features used in this analyses. We know that these paints were not included in this version of the spectral umixing algorithm because the data were only recently available in early 2017 (H. Cowardin, private communication).

Such obvious discrepancies could be attributed to the following methodology changes. First, a spectral unmixing model could be made to have machine learning or give sufficient leverage to the user to eliminate solar cells in those cases where there should not be any. Second, that computing power that can utilize the whole spectral database at once is necessary in future analyses. Third, that a rocket body may display significant properties of Kevlar (motor case) and carbon/carbon (nozzle) and paint that are not represented in the current material database. Thus, the solar cells, while not accurate, could be a stand-in for these other materials.

4.4 Single Order versus Stitched Spectra

What one is supposed to do with the 3-grism spectra is to stitch the three orders together to form continuous spectra. It is possible that a full spectrum gives a more complete understanding of the material properties of these objects. We plot a SSN 16274, an HS 376, and spectra in Fig. 8 for comparison with those of Fig. 2. The results in Fig. 8 are stitched spectra from data on a single night. The stitched spectra, in this case, has a higher percentage error, 0.01%, than the best fit from an individual order of the same object, 0.008%. In a comparison of the percentage errors of the individual order fits for various objects to the percentage errors of the stitched spectra of those same objects, the individual order fits have a factor of two smaller percentage errors than the percentage errors of the fits of the stitched spectra.

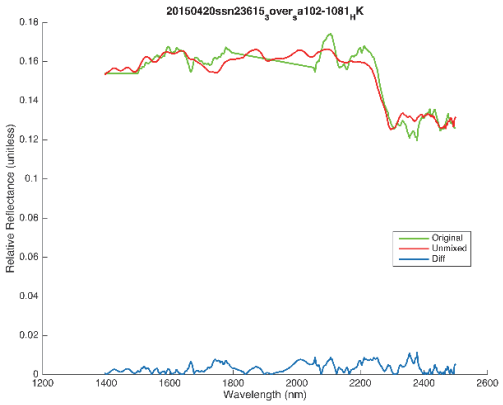

Figure 6. Spectral data from SSN23615, an IUS second stage rocket body, with the HK grism. Green line is the original data, red line is the model fit to the data, and blue is the difference between the green and red lines. The percent error is 2.7%.

Figure 7. An IUS second stage rocket body as it would likely appear on-orbit. Credit: The Boeing Company (composite by D. Shoots, HX5—Jacobs JETS contract)
We can also compare how the model fits a single order fits from one night compared to an averaged spectra of the same order. The two objects, SSN16274 and SSN 27400, were both successfully fit with a one night and multiple night stitches. The multiple night stitches in both cases produced a fit with a worse percentage error but only by an increase of 1%. For SSN16274, this increase is from 0.01% to 1%. For SSN27400, this increase is from 9% to 10%.

We can also compare how the model fits a single order fit from one night compared to averaged spectra of the same order. The two objects, SSN16274 and SSN 27400, were both successfully fit with a one night and multiple night stitches. The multiple night stitches in both cases produced a fit with a worse percentage error but only by an increase of 1%. For SSN16274, this increase is from 0.01% to 1%. For SSN27400, this increase is from 9% to 10%.

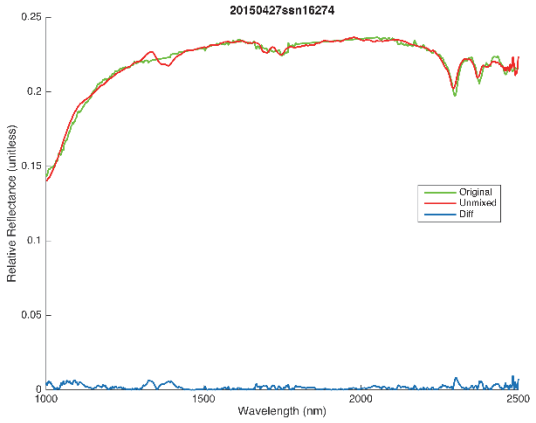

Figure 8. Spectral data from SSN16274 that stitches the three grisms together. Green line is the original data, red line is the model fit to the data, and blue is the difference between the green and red lines. The percent error is 0.01%. From Fig. 2, this percentage error is similar to the percentage error of these stitched spectra.

4.5 Comparison to Previous Study That Used NASA Infrared Telescope Facility Data

A previous study utilizing the same model but with NASA Infrared Telescope Facility (IRTF) data [7] is compared with the results of these UKIRT data. Both studies were infrared based and both studies observed similar (sometimes the exact) objects. IRTF is one continuous spectra without the various grism orders like the UKIRT data. Despite these data differences, the model fits both sets of data well. The percentage error range of their fits was 1%—9%. Eight objects were observed and modeled in this study and in [7]. Seven of the eight objects have similar model composition results and similar percentage errors. The model composition of our study seems to have more materials. This result can be most easily explained by the increase in spectral resolution achieved with UKIRT compared to IRTF. SSN21648 debris has more material components in the IRTF result compared to the UKIRT result. The percentage error of the fit model is higher in the UKIRT study, 10%, than the error in the IRTF study, 1%.

5 CONCLUSIONS

Spectral data taken at UKIRT during 2015 were shown and compared to a constrained linear least squares model using common spacecraft materials. The data collected using the UIST infrared spectrograph cover the wavelength range 0.7-2.5 μm. With UIST data, one can achieve a greater spectral resolution to identify narrower spectral features associated with materials. Overall, data were collected on 17 different orbiting objects at or near the GEO regime. Three of the objects were debris pieces, 1 was a rocket body, and 13 were spacecraft.

The dominant material found was solar cells. Such a finding works well with modeling various spacecraft but does not work well with the rocket body and debris pieces.

The finding of solar cells when modeling rocket bodies and debris pieces suggests two possible avenues at issue with the current model. First, the model does not contain the materials shown in the remote samples. Second, the methodology of the program could be expanded to eliminate the possibility of using certain materials for certain objects, either through a more intelligent algorithm or user control.

With these findings from our preliminary work, the following future work can be conducted. First, adding more laboratory material reflectance samples into the model that can better address the components of both rocket bodies and ejected debris. Due to the wide variation of materials used on space objects, coatings applied to those materials, and space environmental effects while on orbit, having a perfect match between laboratory data and remote data would be impossible. However, the inclusion of more materials into the model and including space environmental and material degradation effects as well will increase the likelihood of determining the material types of these orbiting objects. Second, developing a more robust spectral unmixing algorithm is warranted. A subset of the material database was used due to restrictions in computer capabilities and time. The use of a computer cluster, for example, would allow the full use of the materials database. Further coding development of the spectral unmixing algorithm could lead to better performance as well as machine learning so that the algorithm is choosing the subset of materials. Tertiary topics include subjects like adding more noise to the model such as surface roughness, examining the phase angles in conjunction with the spectra, and removing the water features from the laboratory data.

6 ACKNOWLEDGEMENTS

UKIRT is supported by NASA and operated under an agreement among the University of Hawaii, the

University of Arizona, and Lockheed Martin Advanced Technology Center; operations are enabled through the cooperation of the East Asian Observatory.

7 REFERENCES

1. Ramsay Howat S.K., *et al.*, 2004, "The commissioning of and first results from the UIST imager spectrometer", In Proc Spie 5492, UV and Gamma-Ray Space Telescope Systems, eds. Hasinger G, Turner M.J., p. 1160.
2. Abercromby, K.J., *et al.*, Reflectance Spectra Comparison of Orbital Debris, Intact Spacecraft, and Intact Rocket Bodies in the GEO Regime, *European Conference on Space Debris*, April 2009.
3. Currie, M. J. *et al.*, Starlink Software in 2013, Astronomical Data Analysis Software and Systems XXIII. Proceedings of a meeting held 29 September – 3 October 2013 at Waikoloa Beach Marriott, Hawaii, USA. Edited by N. Manset and P. Forshay ASP conference series, vol. 485, 2014, p. 391.
4. ORAC-DR is copyright 1998-2003 PPARC and distributed by Starlink. http://www.ukirt.hawaii.edu/observing/cookbooks/spectroscopy_reduction_cookbook.html
5. Farnham, T., Schleicher, D., & A'Hearn, M. 2000, Icarus, 147, 180.
6. Rapp, J., Identification of Orbital Objects by Spectral Analysis and Observation of Space Environment Effects, Master's Thesis, California Polytechnic State, San Luis Obispo, September 2012.
7. Abercromby, K., Buckalew, B., Abell, P., and Cowardin, H., Infrared Telescope Facility's Spectrograph Observations of Human-Made Space Objects, *Proceedings of the Advanced Maui Optical and Space Surveillance Technologies Conference,* 2015.